

We are IntechOpen, the world's leading publisher of Open Access books Built by scientists, for scientists

6,900

Open access books available

186,000

International authors and editors

200M

Downloads

Our authors are among the

154

Countries delivered to

TOP 1%

most cited scientists

12.2%

Contributors from top 500 universities



WEB OF SCIENCE™

Selection of our books indexed in the Book Citation Index
in Web of Science™ Core Collection (BKCI)

Interested in publishing with us?
Contact book.department@intechopen.com

Numbers displayed above are based on latest data collected.
For more information visit www.intechopen.com



Perfusion Based Functional MRI

Luis Hernandez-Garcia and Hesamoddin Jahanian

Additional information is available at the end of the chapter

<http://dx.doi.org/10.5772/28969>

1. Introduction

In this chapter, we will discuss the perfusion imaging for functional MRI experiments as an alternative and complementary technique to the conventional Blood Oxygenation Level Dependent (BOLD) effect. We begin by discussing the motivation behind the development of perfusion based functional MRI techniques. In order to do so, we briefly review the underlying relationship between the brain's vasculature and neuronal activity. Increases in neuronal activity result in metabolic increases, which in turn elicit a local, complex, vasodilatory response. With this physiology in mind, we will discuss the advantages and disadvantages of perfusion MRI and BOLD imaging, and which situations are appropriate for each technique. We will discuss how the types of artifacts and noise characteristics present in each technique determine its applicability.

We will then survey a few examples of ASL based fMRI studies. These typically include clinical studies of pathological conditions, longitudinal studies of cognitive function and studies requiring sustained periods of the condition or state of interest (i.e., greater than 30 seconds).

We then proceed to survey the wide array of current techniques available to image cerebral perfusion, including non-MRI techniques. We will describe in broad strokes the basics of PET and SPECT imaging and the use of paramagnetic tracer injections in MRI to map cerebral perfusion. However, we will narrow our focus down to arterial spin labeling (ASL) techniques, which use the water in the arteries as a tracer by labeling it with radiofrequency pulses. Because of ASL's ability to image perfusion dynamically as well as quantitatively, this technique will be the main focus of this chapter.

We will discuss the technical aspects of ASL techniques by first describing the physics of the labeling process and the different labeling schemes available. Here, we will discuss the advantages and disadvantages of each of these strategies in greater detail.

Next, we will discuss the requirements for image acquisition following the labeling period. We will give a brief survey of different image acquisition schemes that are typically used in the ASL literature. While slower non-echo planar techniques can be used for perfusion measurements at rest, functional imaging applications typically require faster, single-shot, echo-planar techniques. 3D acquisition techniques are also gaining prominence in ASL imaging because of signal-to-noise advantages, but they are often accompanied by blurring artifacts if not implemented properly.

We will then proceed to discuss the technical considerations for the analysis of ASL based functional MRI. We divide this section into the *detection* of perfusion changes due to brain activity and the *quantification* of perfusion from the ASL signal.

Linear regression techniques are typically used for detection of activation in ASL data, just as with BOLD data. However, ASL techniques typically rely on the subtraction of images acquired following a labeling pulse from control images that are free of label, in order to extract the perfusion information. As we will discuss in greater detail, there are several subtraction schemes that can be used to isolate the perfusion signal from the raw data. Each of these schemes has an effect on the content and properties of the resulting perfusion weighted signals. We will describe methods to leverage those statistical properties in order to maximize the statistical power of the analysis.

We then address the question of quantifying perfusion from the ASL images. We will discuss the tracer kinetics theory necessary for quantification, and we discuss strategies for quantifying perfusion from time-series data where the perfusion level is changing due to a known stimulation paradigm. In particular, we will discuss how the parameter estimates obtained in the same linear regression procedure used for signal detection can be used to obtain quantitative measures of perfusion both at baseline and perfusion increases due to neuronal activation.

2. Why perfusion fMRI?

Blood Oxygenation Level Dependent (BOLD) contrast fMRI is currently the dominant technique for functional imaging and has yielded a wealth of information about brain function. The observed BOLD contrast arises from a combination of several indirect phenomena that correlate with neuronal brain activation, such as increases in blood volume and perfusion and a decrease in the concentration of deoxy-hemoglobin, that causes the observed BOLD signal intensity to increase in the active area. However, this signal increase is a non-linear function of many physiological parameters as well as the scanner's own characteristics (Boynton, Engel et al. 1996; Buxton and Frank 1997; Buxton, Wong et al. 1998; Vazquez and Noll 1998). As a consequence, BOLD imaging results are typically reported as unitless statistical significance maps without a clear, quantitative, physiological interpretation.

One issue plaguing the BOLD effect technique is that, since the BOLD effect is based on sensitivity to local changes in magnetic susceptibility, artifacts due to susceptibility gradients

are also greatly exacerbated. These artifacts are especially problematic in areas of the brain that lie near air spaces, such as the roof of the mouth, nose and ear canals, as well as the sinuses (Bandettini, Wong et al. 1992; Kwong, Belliveau et al. 1992).

The structure of the drift noise within a session has been shown to be autoregressive (Lund, Madsen et al. 2006) and difficult to remove or model. Furthermore, the height and shape of the BOLD response depend on the baseline perfusion and metabolic levels, and thus effects of interest can be confounded by the conditions of the experimental resting state (Cohen, Ugurbil et al. 2002; Mulderink, Gitelman et al. 2002). Thus, noise properties and drift of the BOLD signal make studies with long activation periods nearly impossible, as the effects of interest are confounded with the slow scanner drifts (Smith, Lewis et al. 1999). The same reasons prevent BOLD FMRI studies from answering questions about baseline conditions. For example, what is the effect of a given drug, therapy, or training regimen on the baseline activity of a brain structure of interest? How do the neural substrates of a specific cognitive function change with age?

Hence, there is a clear need for development of alternative and/or complementary *quantitative* methods to BOLD imaging for FMRI. As technology develops, we expect a paradigm shift toward quantitative methods that offer meaningful physiological interpretation and comparison across laboratories.

This is where perfusion comes in. Perfusion is a readily quantifiable physiological parameter, and is easier to relate to neuronal metabolism than the BOLD response. Furthermore, animal studies conducted at high field, and high spatial resolution have indicated that neuronal activity produces perfusion (Cerebral Blood Flow - CBF) changes that are more localized to the parenchyma than the BOLD effect, consistent with the notion that the BOLD effect is more weighted toward draining veins and away from the active tissue (Duong, Yacoub et al. 2002; Pfeuffer, Adriany et al. 2002; Nencka and Rowe 2007; Olafsson, Noll et al. 2008). Thus, a fast, repeatable technique to measure cerebral perfusion *directly* would be very desirable and complementary to BOLD imaging.

We note that recent blood volume imaging techniques, such as VASO (Lu, Law et al. 2005) and AVIS (Vazquez, Lee et al. 2006), hold promise for quantitative FMRI, but they are severely hampered in terms of signal to noise ratio (SNR), temporal resolution, and multi-slice imaging capability in their present state. The corresponding models for quantification require many assumptions and/or multiple measurements per time point. (Gu, Lu et al. 2006; Changwei, Kai-Hsiang et al. 2008; Jin and Kim 2008 ; Christopher, Ronald et al. 2009). Other methods that indirectly measure the rate of oxygen consumption by the brain are also available, but they require ASL data and calibration studies involving hypercapnia experiments (Davis, Kwong et al. 1998; Hoge, Atkinson et al. 1999). Thus, at this stage, they are not practical for dynamic quantitative functional imaging and will not be the focus of this chapter.

3. A survey of quantitative perfusion imaging methods

Blood flow through any organ has been used as an important measure of its health and functionality for a long time (Kety and Schmidt 1945; Lassen and Perl 1979). As such, many techniques have been developed to measure blood flow based on tracer injections. The central idea behind these is always the same: some substance that can be detected easily (i.e. - radioactivity or fluorescence) gets injected somewhere upstream of the organ of interest, either an artery feeding of the tissue, a vein, or directly into the left ventricle of the heart. Then the concentration of the tracer is measured with the appropriate detector as it travels through the tissue of interest. Perfusion can then be calculated from the uptake curve of the tracer in the tissue.

With the advent of new imaging techniques, the detection process was incorporated into the imaging process, as in autoradiography, PET, or SPECT scanners. These imaging modalities use radioactive tracers to generate the raw signals from which the images are reconstructed. Hence, it was a straightforward leap to use the timing information in order to quantify perfusion through the existing tracer kinetic models.

In the case of MRI, perfusion can also be obtained by imaging the passage of a tracer through the tissue. Instead of being radioactive, though, MRI tracers are molecules that change the relaxation rates of blood and tissue – typically gadolinium compounds, such as Gd-DOTA or Gd-DTPA. MRI has the added benefit that it allows for fairly rapid imaging (1-2 seconds for a whole brain volume) so one can sample the wash-in and wash-out of the tracer through the tissue. One can also simultaneously measure the amount of dispersion of the bolus that occurs during the transit from the injection site to the region of interest. Knowledge of this dispersion provides a more accurate estimate of the tissue's perfusion rate. Unfortunately, one can only do one contrast injection at a time, as the tracer takes many hours to clear the body, so it is not a very useful technique for fMRI.

Thus, our focus is on arterial spin labeling (ASL) techniques. The principle behind ASL imaging is conceptually simple. As with other techniques, the measurement consists of measuring the concentration of a tracer as it passes through a tissue of interest. We will discuss the details in more depth later in this chapter, but for now, note that ASL deviates from the usual tracer strategy in two ways. First and foremost, no tracer is injected. Instead, the tracer is “created” inside the arteries feeding the organ by radio frequency (RF) electromagnetic pulses. These pulses are generated by standard MRI coils and invert the magnetization state of the water protons in the blood. After allowing a short period of time for inflow of the tracer into the tissue of interest, an image is collected. Just like in previous techniques, perfusion can be quantified by measuring the signal change due to the tracer – typically by subtracting the image with the tracer from a control image without the tracer. The second important difference is that the tracer used in ASL decays very quickly, since the longitudinal relaxation rate of arterial blood is in the order of 1600 ms. As a result, there is a significant penalty in the signal-to-noise ratio (SNR) but, on the bright side, the experiment can be repeated immediately and as many times as desired. One can think of ASL as a tracer (also referred to as “label” or “tag”) that is

completely non-toxic, rapidly decaying and it can be selectively injected into any artery (Detre, Leigh et al. 1992; Williams, Detre et al. 1992).

4. ASL and functional MRI

Although ASL is still limited by SNR and temporal resolution relative to BOLD imaging, some features of ASL make it a preferable option in many situations. The most important feature of ASL is the ability to quantify perfusion from the signal difference. This poses a significant advantage over BOLD contrast in that it allows the study of absolute baseline activity (i.e. – resting state) without comparison to an active state. This type of measurement is particularly desirable for studies concerned with pathological states, and/or testing the effects and specificity of different drugs. This ability to quantify perfusion is extremely useful in longitudinal studies over scanning sessions, whether involving activation or limited to the resting state. For example, we have used quantitative ASL to study the long-term effects of working memory training on brain activity, both at rest and during the performance of working memory tasks (Jaeggi, Studer et al. 2009).

Another interesting feature is that although the residual variance of an ASL time course within a single run is higher than with BOLD, it has been shown that the variance of non-quantitative ASL studies (i.e., relative CBF) across scanning sessions is dramatically less than that of BOLD, allowing studies that span days or even months (Aguirre, Detre et al. 2002; Wang, Aguirre et al. 2003; Wang, Aguirre et al. 2003). Furthermore, the variance across subjects is also lower in ASL than in BOLD, thus requiring fewer subjects to be scanned per experiment (Tjandra, Brooks et al. 2005).

Arterial spin labeling techniques allow greater flexibility in the image acquisition, especially when examining slow activation paradigms. Hence, they do not require T_2^* weighting and one can use standard Spin Echo imaging to collect the image data, dramatically reducing susceptibility artifacts. Functional imaging studies of the inferior brain structures, such as the basal ganglia, and the orbito-frontal cortex would benefit greatly from such techniques.

5. Some examples of ASL studies

Due to above mentioned properties of functional arterial spin labeling (FASL), it is particularly useful for the study of gradual changes in neural activity, longitudinal and multi-site studies. (N.B. in this chapter, we use the term FASL to indicate ASL time series used for fMRI purposes, but there is no technical difference between FASL and ASL). FASL has been used in several basic and cognitive neuroscience applications. It has been used in many studies to investigate visual, motor and language functions at 1.5T and 3T (Aguirre, Detre et al. 2002; Wang, Aguirre et al. 2003; Kemeny, Ye et al. 2005; Tjandra, Brooks et al. 2005; Leontiev and Buxton 2007; Ances, Leontiev et al. 2008; Chen, Wieckowska et al. 2008; Raoult, Petr et al. 2011) and has been compared to BOLD fMRI (Aguirre, Detre et al. 2002; Chen, Wieckowska et al. 2008; Raoult,

Petr et al. 2011) (Kemeny, Ye et al. 2005) (Tjandra, Brooks et al. 2005) (Hermes, Hagemann et al. 2007) indicating that the intra-individual reproducibility of FASL in terms of the area of activation and activation quantification is comparable to that of BOLD fMRI. FASL however, detects smaller activation volumes than BOLD fMRI but the areas had a high degree of co-localization between subjects. FASL also shows higher specificity compared to BOLD fMRI while maintaining high sensitivity in activation detection in the activated area (Raoult, Petr et al. 2011).

Due to the drift in the BOLD signal, study of slow changes in neural activity using BOLD is quite challenging. FASL is a suitable tool for these studies as well. Motor learning is an example of the gradual changes in the neural activity over time, which cannot be easily assessed using BOLD fMRI. In (Olson, Rao et al. 2006) Olson et al. used FASL to study continuous, gradual changes in neural activity during motor learning. Subjects were required to use four fingers to press keys as quickly and as accurately as possible in response to the presentation of visual cues. Olson et al. reported that subjects performing this task demonstrated a reduction of neural activity in response to motor execution after training as compared to the start of training. Because the change in performance is slow and continuous, it is assumed for this study that the neural correlate of performance improvement during training is a gradual reduction in regional activity. The authors used FASL to detect these neural changes and reported reliable correlations between performance improvements and decreases in blood flow in premotor cortex and the inferior parietal lobe. This study suggests that FASL is a suitable tool for the study of the slow changes in the neural activity resulting from different cognitive tasks.

FASL has also been used in higher level cognitive activation studies. There is an increasing body of evidence pointing to a neurobiological basis of personality. Characterizing the biological bases of personality dimensions is important to explaining individual differences in brain activity associated with more dynamic changes in experience (e.g., a psychotic episode) and cognition (e.g., activation paradigms in functional MRI) (O'Gorman, Kumari et al. 2006). In (O'Gorman, Kumari et al. 2006) O' Gorman et al. explored the biological bases of the major dimensions of models of personality using FASL. In this study, the correlation between personality factors with regional brain function was successfully investigated using FASL. The authors reported associations between perfusion in brain regions (including basal ganglia, thalamus, inferior frontal gyrus, cerebellum and cuneus) and different personality dimensions. These results suggest that variations in perfusion in certain brain regions correlated with variations in personality dimensions may reflect variations in brain function (O'Gorman, Kumari et al. 2006).

FASL provides reliable quantification of absolute cerebral blood flow (CBF) along with excellent reproducibility over long time periods, making ASL a sensitive technique for reliable visualization of brain function during the resting state as well as during task performance. This property allowed Rao et al. (Rao, Gillihan et al. 2007) to employ ASL to investigate the effect of genetic variation of the human serotonin transporter gene on resting brain function of healthy individuals. They studied the alteration of resting brain function in emotion-related regions (including the amygdala and ventromedial prefrontal cortex) in healthy individuals caused by the 5-HTTLPR genotype. Valid and reliable inferences of resting activity for

applications such as this study could not be derived from BOLD fMRI because it only measures *relative* changes in neural activity, and the changes in signal intensity from scanner drift are much larger than the effects of interest.

Also, using ASL, authors (Rao, Gillihan et al. 2007) demonstrated an association of 5-HTTLPR genotype with resting amygdala and ventromedial prefrontal cortex function in the healthy human brain. Such alterations suggest a broad role of the 5-HTT gene in brain function that may be associated with the genetic susceptibility for mood disorders such as depression.

Neuronal modulations found using functional ASL (FASL), such as those reported in (O'Gorman, Kumari et al. 2006) and (Rao, Gillihan et al. 2007), may also be important in interpretation of the different manifestations of BOLD response (which typically rely on the modulation of cerebral hemodynamics for detection of task-induced activation) to a particular stimuli in different groups.

The presence of low frequency signal drift in the BOLD signal impedes using a long task block. This problem makes it difficult to investigate slow processes such as learning, emotion, sustained attention and behavioral states in healthy and clinical populations. Because of its efficacy in longitudinal designs and low frequency paradigms, FASL is a good candidate for these studies. Kim et al. (Kim, Whyte et al. 2006) successfully utilized FASL to study an uninterrupted 6-min continuous performance of the two high-level cognitive tasks (visual sustained attention and verbal working memory) which prior to FASL was only feasible for suboptimal short data acquisition blocks (40-90s). Understanding the neural correlates of these cognition function is very important because sustained attention is also implicated in various clinical disorders including attention deficit hyperactivity disorder, traumatic brain injury, and Alzheimer's disease (Kim, Whyte et al. 2006).

In another study, Rao et al. (Rao, Wang et al. 2007) used FASL and BOLD to measure brain activation patterns associated with natural vision while subjects were freely viewing a cartoon movie. Rao et al. reported that cerebral blood flow increases in multiple visual pathway areas and frontal areas, and decreases in ventromedial frontal cortex and superior temporal cortex during movie viewing compared to resting states. Concurrent BOLD contrast revealed similar but weaker activation and deactivation patterns. This study demonstrates the feasibility of using FASL for imaging both sustained and dynamic effects in neural activation during natural and ecologically valid situations (Rao, Wang et al. 2007).

With excellent reproducibility over long-term time periods, FASL is ideal for imaging a sustained behavioral state, such as stress. Wang et al (Wang, Rao et al. 2005) used FASL technique to measure perfusion changes associated with mild to moderate stress. The authors demonstrated that a positive correlation exists between the change in perfusion induced by the stress task and subjective stress rating in the ventral right prefrontal cortex and left insula/putamen area. This study provides neuroimaging evidence that psychological stress induces negative emotion and vigilance and that the ventral right prefrontal cortex plays a key role in the central stress response.

Pharmacological functional (phMRI) studies are making a significant contribution to our understanding of drug effects on brain systems. Since noise spectrum of arterial spin labeling

signal contains relatively less power at low frequencies, it is particularly useful for phMRI studies in which a change in brain activity is expected over the course of minutes, hours, or days to assess low frequency between- and within-session drug-induced changes (Wise and Tracey 2006) (16). As an example, Gollub et al. (Gollub, Breiter et al. 1998) used FASL to measure neuronal activation during visual stimulation before and after cocaine and saline infusions. The authors used FASL to determine whether acute intravenous cocaine use would change global cerebral blood flow and demonstrated that cortical gray matter cerebral blood flow was unchanged after saline infusion but decreased after cocaine infusion.

These studies demonstrate that FASL can be successfully utilized for the investigation of the cerebral blood flow changes associated with development of human brain, personality, high level cognitive operations, the behavioral states such as attention, natural vision, psychological stress and assessing low frequency drug effects. Increased applications of FASL to the investigation of cognitively impaired populations are expected to follow.

5. ASL methods

Now that we've seen the bigger picture, let's examine the details of carrying out the acquisition and analysis of ASL data. Any ASL sequence is basically made up of a labeling period, during which the inversion label is created, some delay time to allow the label to reach the tissue of interest, and then an imaging pulse sequence where the image is acquired. There may be additional pulses to shape the input function before the acquisition part, and there may be multiple coils involved in some variants, but in general, the structure remains the same. Thus, it is convenient to discuss labeling and imaging schemes independently, as they can be combined in multiple ways.

6. Labeling schemes

There are a number of MRI pulse sequence strategies that can be used to obtain ASL perfusion images. The first class of arterial spin labeling pulse sequences is "Continuous arterial spin labeling" (CASL). In the original continuous ASL formulation, low-power, long pulses (in the order of a second or two) are applied at a plane inferior to the brain. Typically this is below the circle of Willis where the arterial supply to the brain is perpendicular to the labeling plane. As usual, in order to achieve slice selection, the long RF pulses are applied at some frequency offset and in the presence of a slice-selective gradient. These pulses have very different effects on the stationary and the moving spins. While the stationary spins at the labeling plane become saturated and lose phase coherence (essentially destroying their magnetization), the spins that are moving through the labeling plane experience a gradual change of their resonant frequency (recall that the resonant frequency is directly proportional to the magnetic field). The difference between the resonance frequency of the protons and the transmission frequency changes from positive through negative as the spins move through the inversion plane and is zero at the center of it.

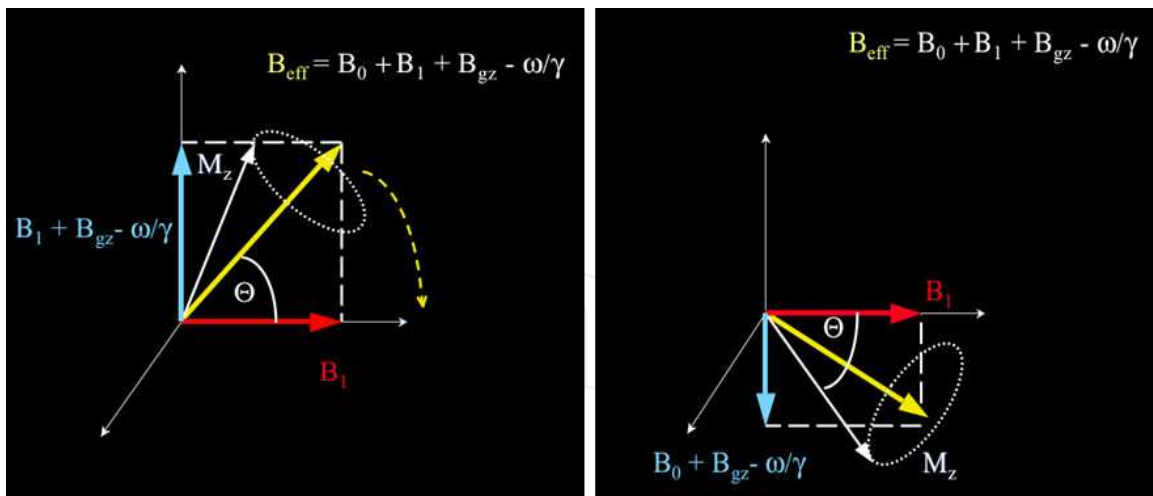


Figure 1. The Adiabatic Inversion Process - 1A – In the rotating frame of reference the magnetic fields due to the scanner’s main magnetic field (B_0), the RF coil’s field (B_1), the slice select gradient (B_z) and the opposing magnetization field add up to an “effective magnetic field” (B_{eff}). The arterial water’s magnetization vector precesses around B_{eff} . 1B- As the spins move, the contribution from the slice select changes from positive to negative. As this happens, the magnetization vector continues to precess around the effective field, resulting in the inversion of the magnetization vector.

Because of this effective “frequency sweep”, the net magnetic field generated by the combination of the main magnetic field (B_0), the applied RF field (B_{1eff}) and the magnetic field resulting from the spin’s precession itself (ω/γ) experiences a rotation from pointing along the direction of the main magnetic field to pointing against it (see figure 1). If this rotation is slow relative to the precession frequency, the effect of the constant RF pulse on these moving spins is to create a “spin-locked” state. This means that the flowing proton’s magnetization processes around the effective magnetic field and follows it as it rotated from pointing up to pointing down.

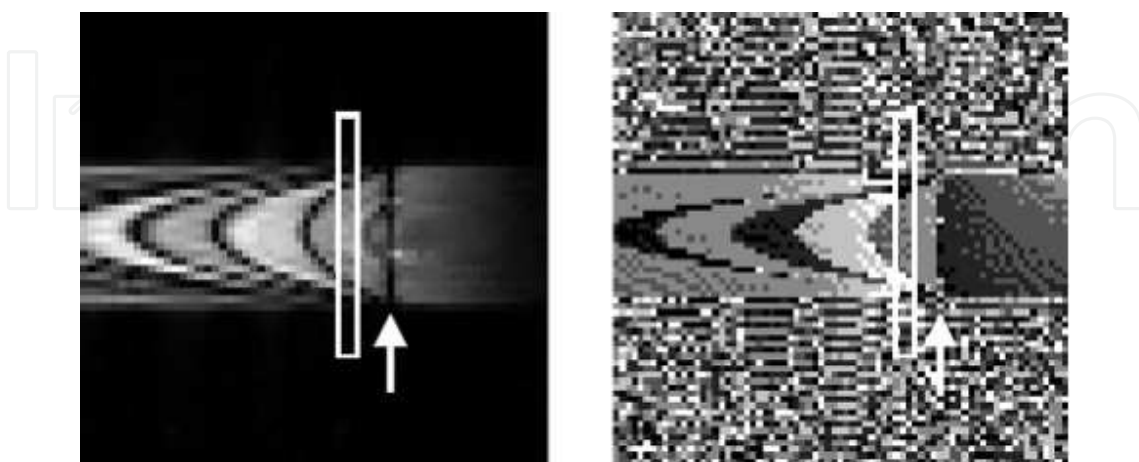


Figure 2. This image shows the magnitude (left) and phase (right) of an image of water flowing through a tube while experiencing adiabatic inversion. The banding pattern reflects periods where the pulses were turned on and off. Figure reproduced from (Hernandez-Garcia, Lewis et al. 2007).

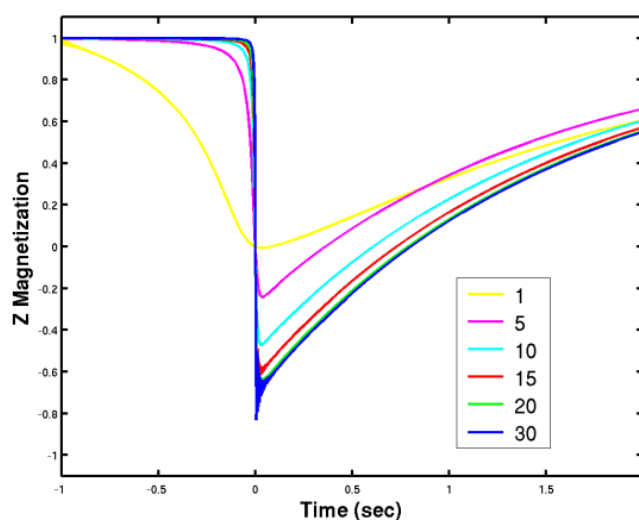


Figure 3. The longitudinal magnetization of the arterial water experiences adiabatic inversion at the labeling plane, then slowly decays back to its relaxed state. This phenomenon depends on a number of factors, such as the velocity of the spins, and the size of the slice select gradient and the RF fields used in the pulse sequence.

As the protons move through the inversion plane, the “effective” field (B_{eff}) to which they are locked rotates from pointing along the direction of the main magnetic field to pointing against it. The end result is that when the flowing spins leave the plane, their magnetization is inverted (figure 2 shows a practical demonstration of this phenomenon). This phenomenon is referred to as “flow driven adiabatic inversion” and is the basis for continuous arterial spin labeling techniques. It is important to note that immediately after inversion, the spins experience T1 relaxation and the label effectively decays in a matter of a couple of seconds, as depicted in figure 3.

The main caveat of continuous ASL is that the long inversion pulses applied at the neck for labeling purposes also produce a significant amount of magnetization transfer (MT) (Detre, Leigh et al. 1992; Williams, Detre et al. 1992) in the spins at the tissue of interest. Briefly, magnetization transfer consists of signal loss during acquisition when it is preceded by RF pulses, even if those are not applied on resonance. As a result of MT, subtracting a tagged image from a control image would indicate not only the perfusion effects but also the degree of magnetization transfer, which is of no interest to the investigator.

This would constitute a major obstacle, but a number of solutions have been devised. The original solution to this problem was to apply an MT preparation pulse with identical properties to those of the labeling pulse before collecting the control image. This preparation pulse was identical to labeling pulse but with a reversed slice select gradient such that the inversion pulse would be centered above the head. In that case, there is only magnetization transfer but no arterial spin labeling. While this works in principle, it is difficult to collect more than one slice at a time while appropriately compensated magnetization transfer symmetrically for all the slices. Another solution was to simply use a separate RF coil for labeling whose field pattern will not reach the brain (Zhang, Silva et al. 1995) (Talagala, Ye et al. 2004) (Hernandez-Garcia, Lee et al. 2004). While this approach works quite well and relatively simple to implement in principle, in practice it requires additional hardware that can be synchronized

with the main MRI scanner's pulse sequence. It is also generally uncomfortable for the subjects to wear the additional neck coil and it can pose some logistical pulses.

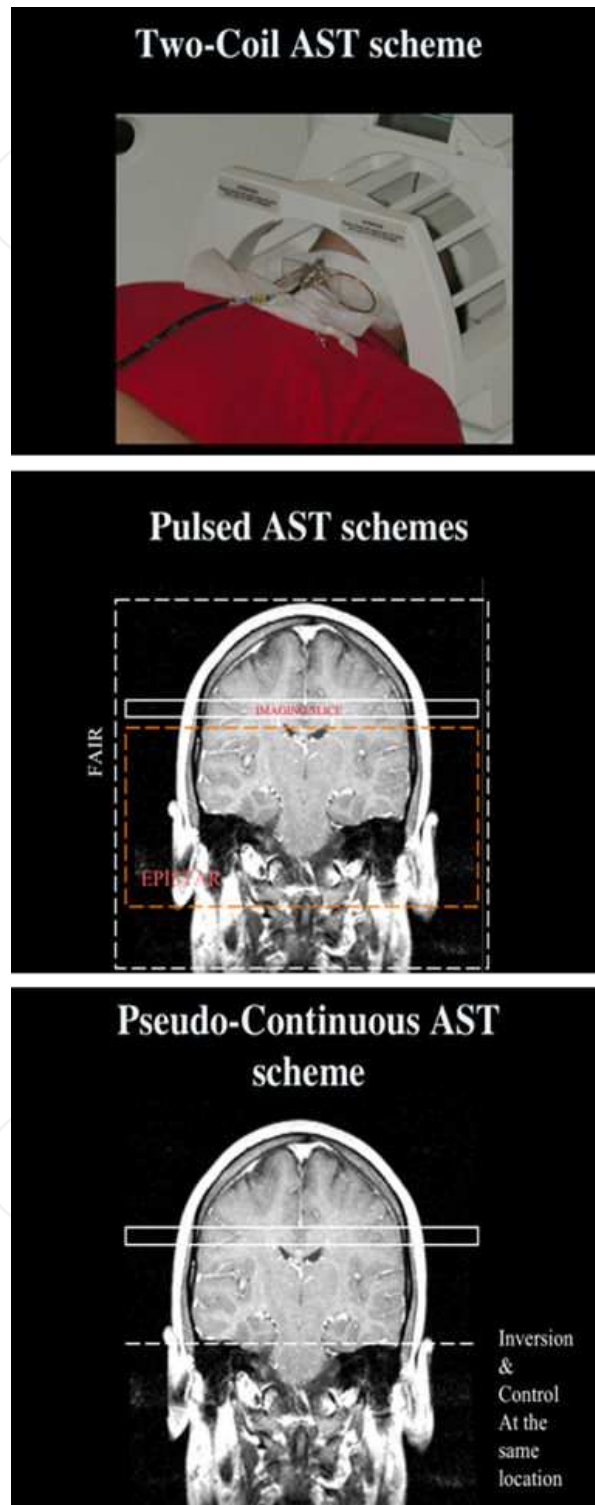


Figure 4. Labeling Schemes - Schematics indicating the relative locations of the inversion types of popular ASL schemes

Several other strategies to overcome the magnetization transfer problem have been tried to overcome this problem, such as amplitude modulated CASL (Wang, Zhang et al. 2005), but the most promising one is to break up the continuous labeling pulse into a train of pulses applied in rapid succession to achieve the same adiabatic inversion effect. In the control case, however, the same pulse train is applied but the phase of every other pulse is shifted by 180 degrees, such that every other pulse “un-does” the flip of the previous pulse. The end result is that both the control and the labeled image receive the same amount of magnetization transfer, the flowing blood’s magnetization gets inverted prior to collecting the labeled image but it remains un-inverted during the collection of the control image. This technique, known as pseudo-continuous arterial spin labeling (PCASL) has greatly facilitated the use of continuous ASL because it addresses the magnetization transfer issue and is relatively easy to implement (Garcia, de Bazelaire et al. 2005; Wang, Zhang et al. 2005; Fernandez-Seara, Wang et al. 2007; Wu, Fernandez-Seara et al. 2007). The caveat is that PCASL is sensitive to magnetic field inhomogeneity (off-resonance) at the inversion plane. This effect can severely affect the efficiency of the labeling process, crippling the technique, and is exacerbated at higher magnetic fields. Fortunately, the loss of inversion efficiency can be recovered by adjusting the phase of the inversion pulses and introducing compensation gradients (Jahanian, Noll et al. 2011).

A second class of arterial spin labeling pulse sequences is “pulsed ASL” (PASL). This strategy is to label a slab containing the arterial supply to the organ of interest with a more standard, short RF inversion pulse and then allow the inverted spins to flow from that slab into the tissue of interest. The difference in signal intensity between the two images is provided by the un-inverted spins that flowed into the imaging slices during the inversion delay. This signal intensity difference can then be readily quantified and translated into perfusion images. This process mimics the injection of a bolus of tracer, rather than a constant infusion, as in the case of continuous ASL.

The simplest form of pulsed ASL is the EPISTAR technique (Edelman and Chen 1998), in which the inversion pulse (typically a hyperbolic secant) applied just below the region of interest followed by a delay to allow the inverted blood to flow into the tissue before collecting the image. Hyperbolic secant pulses are relatively short adiabatic pulses and exhibit no significant magnetization transfer effects, so there is no need for pre-compensation pulses before collecting the reference image. In the FAIR technique (the original pulsed ASL technique) the control image is preceded by an inversion pulse applied over the entire brain, followed by a short delay (Kim 1995; Kim and Tsekos 1997). The tagged image is collected following a similar hyperbolic secant inversion pulse, except that it is applied only over the slices of interest, followed again by the same short delay to allow for inflow of blood into the imaging region. There are many variants on this theme, but perhaps the most popular pulsed ASL technique is QUIPSS which uses additional pulses to saturate the trailing edges of the label, thus producing a clearly defined bolus (Wong, Buxton et al. 1997; Wong, Buxton et al. 1998).

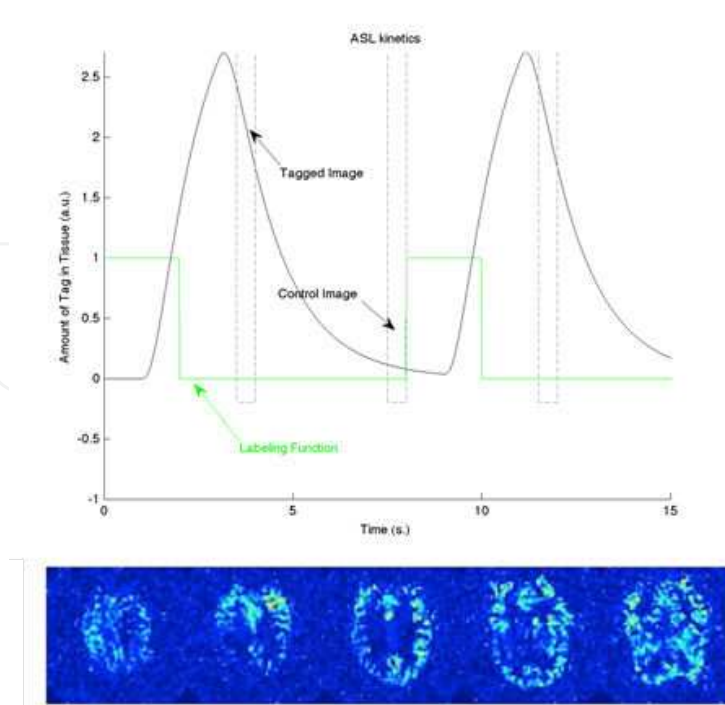


Figure 5. A - The uptake and release of the inversion label is relatively short, so there is only a limited amount of time to collect the images without a significant signal change. While including long post inversion delays reduce the sensitivity to the difference in slice timing, there is still only a limited amount of time to collect the images. If the process takes too long, different slices will have different SNR and sensitivity to perfusion changes from activation. B – This image, originally consisting of 24 slices, shows a noticeable change in SNR between the top and bottom slices. Here we only show slices 6, 9, 12, 15.

Whereas the pulsed approach only requires 1-2 seconds for the label to reach its maximum concentration in the tissue the continuous approach requires approximately 3 seconds before a steady state concentration of tag is reached. However, because of the longer inversion times of the continuous labeling scheme, the amount of tag to be detected is much larger and thus, the SNR of the method is also larger (Buxton, Frank et al. 1998; Wong, Buxton et al. 1998). Thus, the tradeoff between them is primarily one of speed versus SNR.

7. Image acquisition considerations in ASL

Image collection following the spin labeling process can be done in a number of ways, but it is important to take into account the goals of the specific application. As usual in MRI, there is a trade-off between acquisition speed, SNR and resolution.

In clinical and resting state applications, typical ASL scans use more standard image acquisition pulse sequences since the speed consideration is relaxed. Fast spin-echo acquisitions are a popular method because of their insensitivity to off-resonance artifacts and relatively high SNR and speed. For example (Fernandez-Seara, Wang et al. 2005; Fernandez-Seara, Wang et al. 2007) used a 3D GRASE acquisition sequence in conjunction with

continuous ASL in order to boost the SNR of the acquired images in a functional imaging study of the medial temporal lobe.

Functional MRI requires image acquisition speed in order to capture the hemodynamic changes that take place during mental activity adequately. Fast imaging techniques that take advantage of echo-planar and echo-volumar acquisition and parallel imaging allow us to image the whole brain in a matter of a second or two with high spatial resolution. Consider the figure below, which indicates the concentration of tag in the tissue as it is taken up. Unfortunately, the rates at which the flows in and out of the tissue while decaying is such that we are constrained to roughly a half a second to acquire the whole volume.

If one slice is collected at the beginning of the uptake and another toward the end, the perfusion contrast will be vastly different. While one can account for it by including this delay in the quantification scheme, the SNR of the slices can still be significantly different.

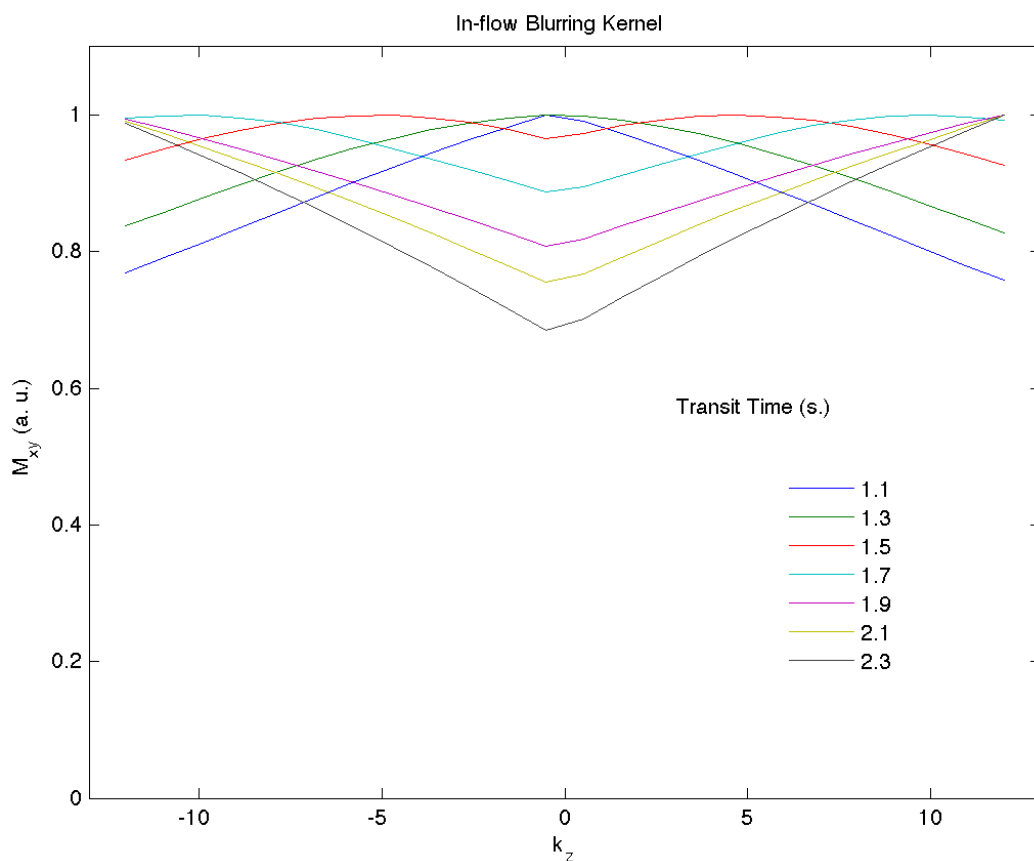


Figure 6. Depending on the transit time of the blood from the labeling plane to the imaging slab, the uptake of the label can induce a mild distortion along the slab-select location (or k_z). Interestingly, this effect can be characterized by a point spread function that acts as either a high-pass or low-pass filter along the k_z axis.

This acquisition time window means that there is a significant constraint in the number of slices that one can get after a single labeling period. For instance, using a fast spiral acquisition typically allows for acquisition of a single slice in at least 25 ms. At this rate one can acquire

20 slices in half a second, which is adequate but requires thick slices of about 6 mm thickness, assuming a 12 cm brain.

In this regard, there is recent interest in the development of 3D echo-planar and echo-volumar acquisition schemes. 3D imaging schemes can ensure the same acquisition delay for the entire imaging volume relative to the labeling period. The SNR of 3D imaging can be greater than 2D multislice because a larger volume contributes to each echo. For example, Gunther et al (Gunther, Oshio et al. 2005) proposed a multi-echo 3D acquisition that allows collection of a k-space plane at each echo. Unfortunately, this acquisition scheme imposes a T2 weighting on each plane of k-space depending on the acquisition order. The result is typically a severe blur of the volume along the z-direction. One can think of this as a blurring filter applied along the slice direction, and the shape of that filter's point spread function (PSF) is that of the T2 decay.

Another 3D alternative is to use multi-shot readouts as in (Talagala, Ye et al. 2004) but these typically require the use of low flip angles to preserve the magnetization throughout all the kz encoding steps. Low flip angles however result in reduction of the available signal. Gai et al (Gai, Talagala et al. 2011) have experimented with an increasing flip-angle schedule starting at 10 degrees that produces a constant signal along kz according to the Ernst formula. This approach produces a flat PSF, but at the cost of SNR. In recent investigation, we have found that a flip angle schedule that starts at 15 degrees and increases with a simple third order polynomial is a good compromise between SNR and blurring along the slice direction. The figure below illustrates this issue by calculating the PSF along the z-direction of different order polynomial flip angle schedules.

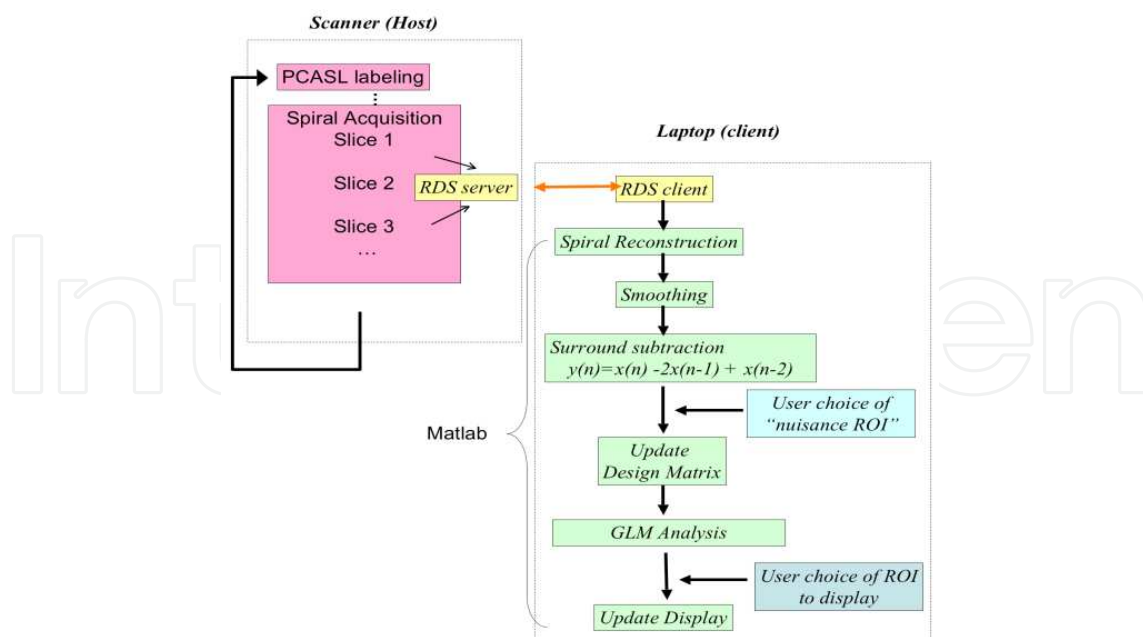


Figure 7. Real Time imaging with ASL requires coordination of the scanner's acquisition with an external computer that "catches" the data as it is generated by the scanner and carries out the analysis within the interval between two images. (Figure from (Hernandez-Garcia, Jahanian et al. 2011))

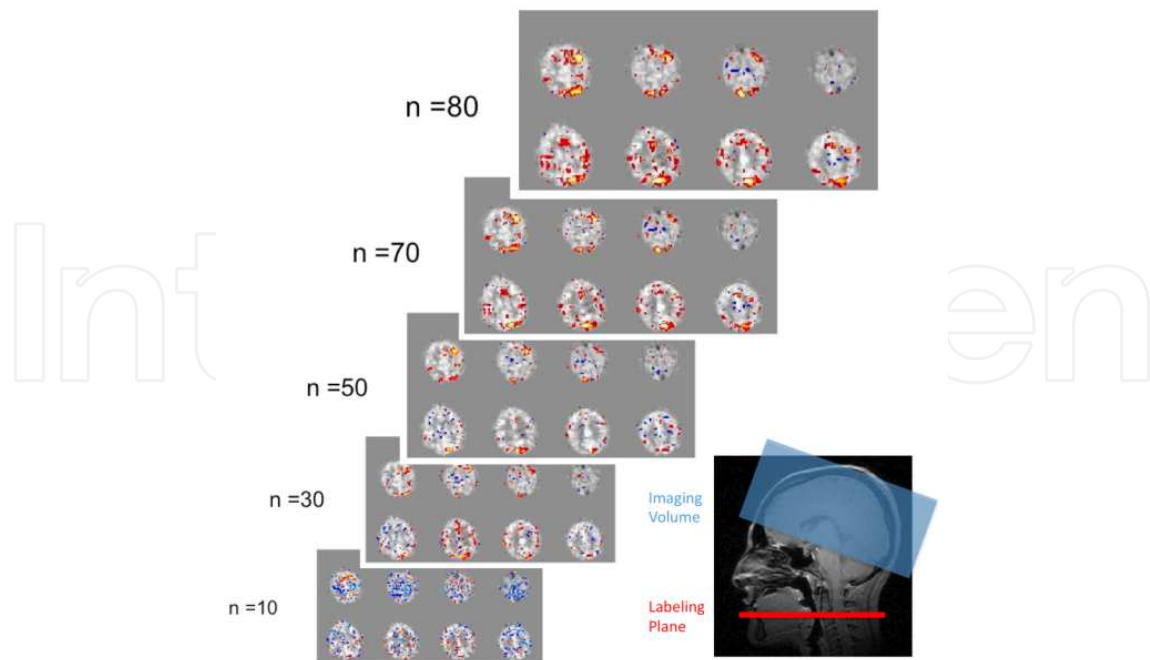


Figure 8. This figure shows an updated view of the real time FASL acquisition during a visuo-motor stimulation paradigm. As one can see, the activation maps evolve over time and become better defined as more data become available. (Figure from (Hernandez-Garcia, Jahanian et al. 2011))

Real-time functional magnetic resonance imaging (rtfMRI) is an exciting extension to conventional fMRI techniques that enables the user to analyze fMRI data as it is being collected. The requisite is that the reconstruction and analysis must be carried out before acquisition of the next image in the time series (about two seconds for standard FMRI). Thus, in rtfMRI the results are immediately available as the subject is being scanned, and can be used to reveal and/or guide the subject's cognitive processes. Thus, by collecting the data in real time, the investigator can fine tune the design's parameters to suit each specific subject (deCharms 2008). One can also design interactive paradigms based on the subject's dynamic functional activity (fMRI biofeedback or brain-computer interface (Yoo, Fairney et al. 2004)). Furthermore, it allows the investigator to determine the subject's compliance during the experiment. Examples of real time FMRI also include studies of the modulation of motor-area cortical activation and emotional processing by the subjects themselves (Yoo and Jolesz 2002; Posse, Fitzgerald et al. 2003; deCharms, Christoff et al. 2004; Phan, Fitzgerald et al. 2004; Caria, Veit et al. 2007).

A number of processing strategies have been developed in order to carry out real time FMRI analysis, such as cumulative correlation (Cox, Jesmanowicz et al. 1995), sliding-window correlations with reference vector optimization (Gembris, Taylor et al. 2000), online general linear model [GLM] analysis (Nakai, Bagarinao et al. 2006). There are also a number of combined methods to collect behavioral, physiological and MRI data while performing near real-time statistical analysis (Voyvodic 1999). The recent advances in computational speed have made it relatively easy to implement any of these analysis methods.

8. Quantifying perfusion from the ASL signal

In the original implementation of continuous ASL, quantification was done by writing the well-known Bloch equations that describe the longitudinal magnetization with one modification: the authors included terms to account for the inflow of arterial blood and outflow of venous blood. (Recall that the Bloch equations describe the behavior of a magnetization vector in the presence of magnetic fields such as the ones present in an MRI pulse sequence Please see textbooks like Haacke's (Haacke 1999) or Bernstein (Bernstein, King et al. 2004) for an introduction). Like this $\frac{dM_{tissue}(t)}{dt} = f \cdot M_{art}(t) - \frac{f}{\lambda} \cdot M_{tissue}(t) - \frac{M_{tissue}(t)}{T_1}$

Here, $M_{tissue}(t)$ would be the longitudinal magnetization of the tissue protons. $M_{art}(t)$ is the incoming arterial magnetization. In the control image it would be positive, but in the labeled image, it would be negative. Note that this must be adjusted to reflect the efficiency of the inversion efficiency (α) and its decay during transit time from the labeling plane to the tissue (Δ). Hence, $M_{art}(t) = (2\alpha e^{-(\Delta/T_{1art})})M_{art}(0)$.

T_{1art} and T_1 are the longitudinal relaxation rates of the arterial blood and the tissue. The parameter λ is blood brain partition coefficient and it relates the concentrations of label in blood and tissue at equilibrium. The key parameter is f , the perfusion rate that describes the rate at which water moves in and out of the tissue. By writing the steady state solutions for this equation in the case of control and tagged images, one can solve for f .

An equivalent but perhaps more generalizable approach was presented by Buxton et al (Buxton, Frank et al. 1998) in which they treated the ASL experiment as a standard tracer kinetics experiment. In this formulation, the concentration of "label" in the tissue, C_{tissue} is given by the subtraction of control and tagged images, and can be modeled as a linear system. In that case, the observed signal difference between control and tagged images is the convolution of an input function with a system function.

$$C_{tissue}(t) = f \cdot M_{art}(t) * [r(t)m(t)]$$

In this case, the input function is a fraction of the arterial blood (determined by the perfusion rate, f). The system function is a combination of the tissue "retention" function, e^{-ft} , which describes how the label clears away with an exponential decay, and also the T_1 decay function of the tag in the tissue, e^{-t/T_1} .

In subsequent work the pulse sequence's timing parameters, including the TR, duration of the tagging period (ω), post inversion delay (τ) and transit time (δ) were taken into account to yield the following equation relating the subtraction image (ΔM) to the perfusion rate. If the post inversion delay is longer than the transit time, the perfusion rate can be calculated by

$$f = \frac{\lambda \cdot \Delta M \cdot R_{1app}}{\left(\frac{M_{control}}{1 - e^{-TR \cdot R_1}} \right) \cdot 2 \cdot \alpha \cdot e^{-\delta \cdot R_{1a}} \left(e^{(\delta - \omega) \cdot R_{1app}} - e^{(\delta - \tau - \omega) \cdot R_{1app}} \right)}$$

Note that R_1 is simply the reciprocal of the T_1 relaxation rate (or $1/T_1$) used for convenience. In keeping with the notation of the authors, R_{1a} refers to the relaxation of arterial blood and R_{1app} refers to the apparent relaxation rate of the tissue.

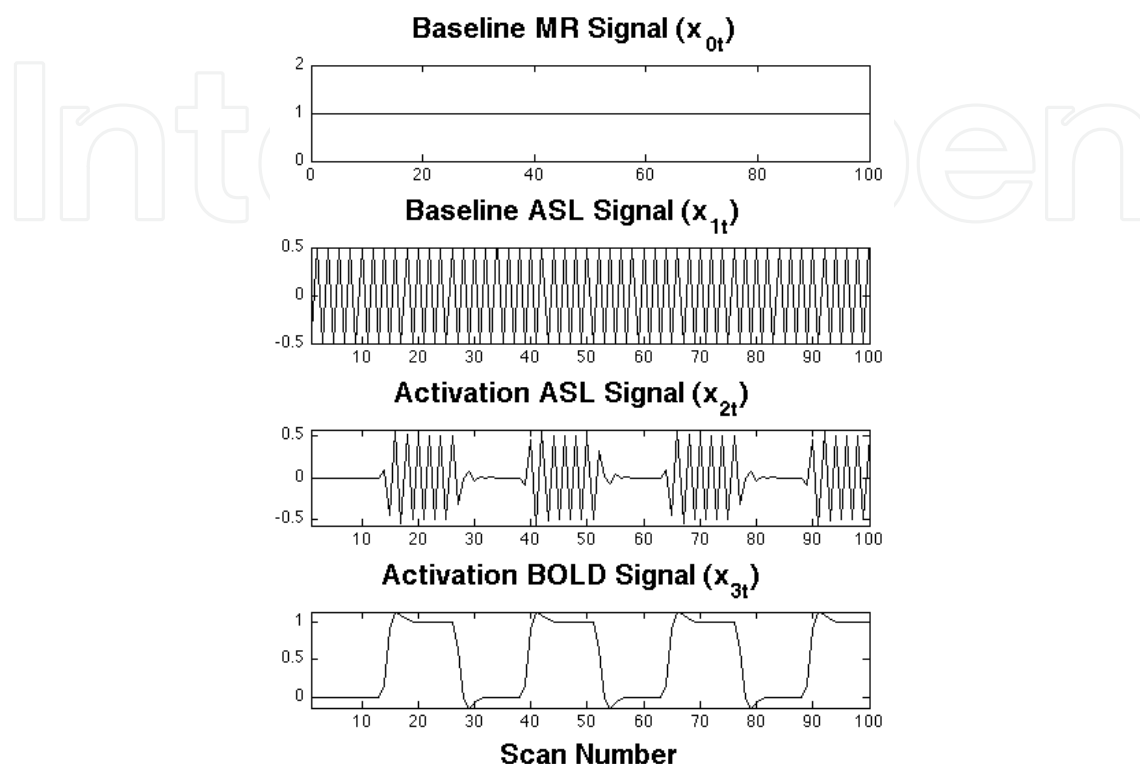


Figure 9. The regressors in a design matrix for a simple functional ASL experiment (only two conditions) include both the usual baseline and BOLD effects (regressors 0 and 2). In order to capture the variance due to resting and activation blood flow, we must include regressor 1 and 3, which are modulated by the presence of the arterial label. Reproduced from (Hernandez-Garcia, Jahanian et al. 2010)

On a practical note, R_{1a} and R_{1app} may vary from subject to subject when dealing with clinical populations or across age groups, so in those cases, it is important to make those measurements separately and use the measured values in the calculation. In the healthy subjects typically used for fMRI research, this is not so much of a factor and literature values are typically employed for the relaxation rates.

9. Quantification of perfusion in FASL data

While the above framework is useful for situations where perfusion is constant, it's more challenging to quantify dynamic perfusion changes as in the case of fMRI experiments. The very slow sampling rate of ASL makes it difficult to get perfusion values during the transitions between active and resting states, so investigators are often forced to settle for collecting only a few perfusion measurements obtained at the baseline and a few measurements at the plateau of the activation, and none from the transition. Unfortunately, this reduces the number of

samples available for quantification, which can be fatal in a low SNR technique like ASL. Furthermore, it precludes event-related fMRI, where there is not much of a plateau of activation.

In order to overcome this problem, one can formulate a general linear model (GLM) that specifies BOLD and ASL effects. One can then estimate the coefficients of this model and translate them into meaningful, quantitative measures of perfusion by using standard tracer kinetic models. This concept is based on the simple realization that the difference images used in ASL quantitative models have a direct relationship to the coefficients (or amplitudes) of the regressors or the general linear model. Since estimation of a general linear model is the standard way of analyzing fMRI data by the bulk of the functional imaging community, this approach constitutes a natural next step in the analysis.

For example, let us consider an ASL fMRI experiment with a baseline condition and a single activation condition with tag and control ASL images acquired in each. One such experiment can be characterized by a linear model, as previously described (Mumford, Hernandez-Garcia et al. 2006). Let y_t be the time course (a vector) of image intensity at a particular voxel obtained from an ASL experiment. In Fig. 9 are the regressors of a simple ASL design matrix representing the linear model

$$y_t = \beta_0 + \beta_1 x_{1t} + \beta_2 x_{2t} + \beta_3 x_{3t} + \varepsilon_t$$

for time $t=1, \dots, n$. The first regressor, the baseline vector $x_{0t} = 1$ and its coefficient parameter, the scalar β_0 , indicate the baseline signal, and can be interpreted as a measure of spin density. The second regressor x_{1t} describes the baseline difference between control and tagged images ($\Delta\Delta M$) and thus its amplitude, β_1 , is indicative of baseline perfusion. The third regressor x_{2t} with its regression coefficient β_2 describes differences between control and tagged images (ΔM) due to activation, and the fourth regressor x_{3t} with its regression coefficient β_3 describes the BOLD effect changes. By realizing that the amplitude of the oscillation (β_2) induced by the ASL scheme corresponds to the difference between control and tagged images, perfusion can be computed dynamically by translating the coefficient parameter estimates of the oscillations into the appropriate control-tag differences.

Quantification of perfusion effects in continuous ASL data without background suppression can be done directly by adapting the same kinetic model by Wang et al (Wang, Alsop et al. 2002) that we discussed in the previous section. The ΔM parameters are replaced with the GLM parameter estimates as follows

$$f_{effect,t} = \frac{\lambda \cdot R_{1app} \cdot \hat{\beta}_{effect}}{\left(\frac{\hat{\beta}_0}{1 - e^{-TR/T_1}} \right) \cdot 2 \cdot \alpha \cdot e^{-\delta \cdot R_{1a}} \cdot \left(e^{(\delta - \omega) \cdot R_{1app}} - e^{(\delta - \tau - \omega) \cdot R_{1app}} \right)} \cdot x_{effect,t}$$

where $\hat{f}_{effect,t}$ is the estimated perfusion change due to the effect of interest, α is the inversion efficiency, $x_{effect,t}$ is the regressor for the effect at time t , $\hat{\beta}_{effect,t}$ is the coefficient parameter estimate of the regressor representing the effect of interest (for example, the amplitude of the perfusion changes due to activation in the above model are captured by β_2), $\hat{\beta}_0$ is the baseline state signal (T_1 -weighted spin density), λ is the blood brain partition coefficient, R_1 , R_{1a} , R_{1app}

are the longitudinal relaxation rates of arterial blood, tissue, and tissue in the presence of perfusion. The term δ is the arterial transit time, while TR , w , and τ are repetition time, post labeling delay, and labeling duration.

As previously noted (Wang, Alsop et al. 2002), when long post-inversion delays (w) are used, the equation becomes insensitive to changes in arterial transit time. Note also that the sign of $\hat{\beta}_{effect}$ can be positive or negative depending on the acquisition order of the control and tagged pairs.

But, what about the error on those parameter estimates? Both Ordinary and Generalized Least Squares estimation yield estimates of the linear model's parameters as well as their variances. Thus, the same relationship can be used to derive the standard deviation of the estimates in perfusion units. In order to calculate the variance of the estimated *perfusion* effects, we propagate the errors of the relevant coefficient parameter estimates through the kinetic model.

Propagation of error can be calculated in a straightforward way from the partial derivatives of the model relative to the coefficient parameters of interest (Bevington and Robinson 2003). We refer the readers to the article by Hernandez-Garcia et al (Hernandez-Garcia, Jahanian et al. 2010) for the derivation.

We have seen that instead of calculating a perfusion time series one image at a time, we can make a linear model of what that perfusion time series should be, and then estimate the corresponding coefficients and their variance. If the model is accurate, this yields much better estimates of the perfusion time series. To illustrate this point, figure 10 shows the perfusion time courses at a given voxel obtained from the traditional method versus the GLM method. Since the residual variance estimates are reduced, the activation maps and residual variances are greatly improved, as illustrated in figure 11.

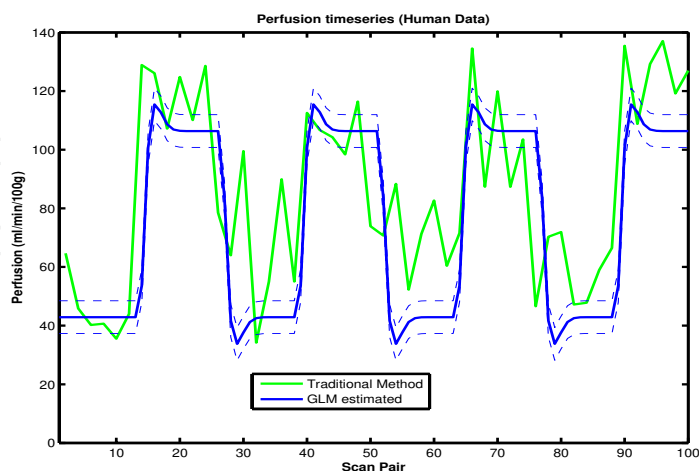


Figure 10. The green line shows the individual perfusion time series calculated at each individual time point. The propagation of errors through the equation makes the result noisy. However, by using all the data at once to estimate the coefficients of a linear model, one can also obtain such a time course if the activation paradigm is known. Reproduced from (Hernandez-Garcia, Jahanian et al. 2010)

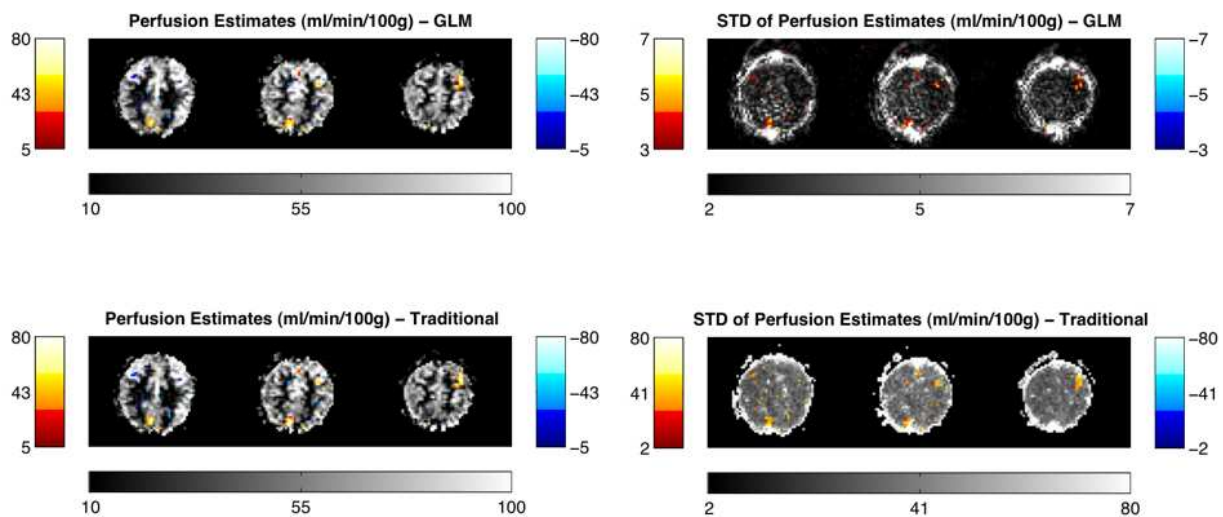


Figure 11. By translating the coefficients of a GLM into perfusion estimates, the residual variance is greatly reduced in comparison to calculating the perfusion time series first and then estimating a general linear model. The result is more accurate activation maps. As with all linear models, one must know the activation paradigm a priori. Reproduced from (Hernandez-Garcia, Jahanian et al. 2010)

10. About the subtraction of the ASL time series

As we have described earlier, the perfusion information in the ASL images is contained in the subtraction of tagged images from control images, which are previously acquired in an alternating order. While differencing the image time course reduces the degree of autocorrelation in ASL data (Aguirre, Detre et al. 2002 ; Liu and Wong 2005) and is widely used, this topic deserves some attention, as there are multiple options available with their corresponding side effects.

In its simplest form, subtraction is done by “pairwise differencing” in which every two images is used to obtain a single perfusion image. As a result, the raw data are no longer auto-correlated, but they are also sub-sampled severely and, consequently, aliasing can occur. By this sub-sampling one also gives up almost half of the degrees of freedom in the analysis, so it translates into a major loss of power. There are other ways to difference the data, however. For example, one can make a “running subtraction” in which one would subtract from every image the previous one, but reverse the sign of the subtraction at every image. Similarly, one would subtract from every control image the average of the two neighboring tagged images (i.e., “surround subtraction”). In this case, only two degrees of freedom are lost, and the data are still whitened. The caveat is that all these differencing processes have a smoothing effect on the time course so fast changes in perfusion are dampened, and we may not be able to observe them. The “sinc subtraction” scheme consists of interpolating the value of the control images at the time of acquisition of the tagged images and, likewise, interpolating the tagged images to obtain their value at the time of the control images. The two up-sampled time courses are then subtracted from each other.

pairwise

$$y_2[m] = y_c[m] - y_t[m] \Leftrightarrow D_2 = \begin{pmatrix} 1 & -1 & & 0 \\ & 1 & -1 & \\ & & \ddots & \\ 0 & & & 1 & -1 \end{pmatrix}$$

running

$$y_3[n] = (-1)^n \cdot (y[n] - y[n+1]) \Leftrightarrow D_3 = \begin{pmatrix} 1 & -1 & & & 0 \\ & -1 & 1 & & \\ & & 1 & -1 & \\ & & & \ddots & \ddots \\ 0 & & & & -1 & 1 \end{pmatrix}$$

surround

$$y_4[n] = (-1)^n \cdot (2y[n] - y[n+1] - y[n+2]) \Leftrightarrow \begin{pmatrix} 1 & -2 & 1 & & & \\ & -1 & 2 & -1 & & \\ & & 1 & -2 & 1 & \\ & & & \ddots & \ddots & \ddots \\ & & & & -1 & 2 & -1 \end{pmatrix}$$

Figure 12. Examples of differencing matrices that can be used for functional ASL. Whether we use an ordinary least squares (OLS) approach on differenced data or a generalized least squares approach (GLS) on raw data can make a significant difference in the statistical power of the analysis. It's not important for blocked designs, but in the case of event related designs, whose frequency content is relatively higher, it makes a significant difference, whether the inter stimulus interval (ISI) is randomized or not. Reproduced from (Mumford et al. 2006)

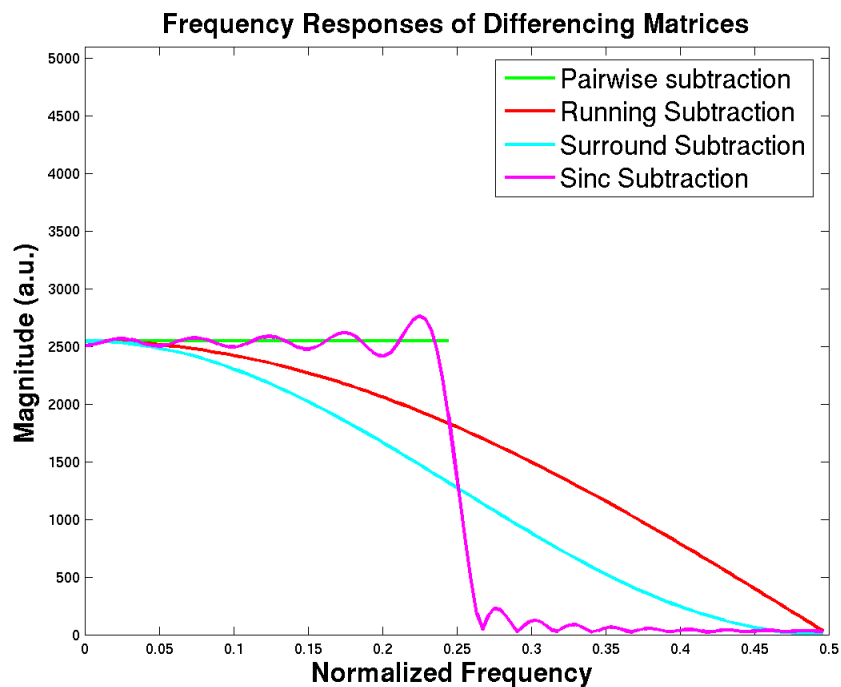


Figure 13. The effect of the differencing process on the frequency content of the ASL signal. Reproduced from (Mumford, Hernandez-Garcia et al. 2006).

From a signal processing point of view it is useful to note that the differencing schemes can be thought of as multiplying the time course by a “differencing matrix”. Figure 12 shows some of the differencing matrices that are commonly used. This differencing process, in addition to isolating the perfusion weighting, also behaves like a filter applied to the data and frequency responses can be computed accordingly. For example, figure 13 shows the filtering effect on the frequency content by several differencing “filters”.

Those frequency responses can be derived analytically for a given input $y[n]$ whose discrete Fourier transform is given by $Y(e^{j\omega})$, yielding the equations in Table 1.

Note that pairwise subtraction and sinc subtraction do not have a straightforward linear response since they involve down-sampling the data. In both of those cases, the down-sampling process causes the top half of the frequency spectrum to alias into the bottom half before the filtering process. In terms of their frequency response, they are very similar except for the imperfections of the sinc kernel used in the implementation. In terms of detection and statistics, sinc subtraction preserves greater degrees of freedom than pairwise subtraction, which reduces the number of time points by half.

Type of Differencing		Fourier Domain Expression
D_1	No subtraction	$Y_1(e^{j\omega}) = Y(e^{j\omega})$
D_2	Pairwise subtraction	$Y_2(e^{j\omega}) = 0.5 \cdot [Y(e^{j\omega/2})(1 - e^{j\omega/2}) + Y(e^{j(\omega+2\pi)/2})(1 - e^{j(\omega+2\pi)/2})]$
D_3	Running subtraction	$Y_3(e^{j\omega}) = Y(e^{j(\omega+\pi)})(1 - e^{j(\omega+\pi)})$
D_4	Surround subtraction	$Y_4(e^{j\omega}) = Y(e^{j(\omega+\pi)})(-1 + 2e^{j(\omega+\pi)} - e^{2j(\omega+\pi)})$

Table 1. Frequency Responses of the differencing schemes

With that in mind, it is important to take the differencing matrix into account when constructing a general linear model for analysis. In the previous section we constructed a model that contained both BOLD effects and ASL effects (see figure 9). Let X represent the corresponding design matrix. We can then re-write the general linear model equation with an additional Differencing matrix, like this:

$$DY = DX\beta + D\varepsilon.$$

It is crucial to note that whatever we do to the data, we must also do to the model if that model is to be as accurate as possible. Hence we difference the data, we must also difference the model, including the noise term. If no differencing is applied, the matrix D can be the identity.

At this point, the objective is the same as in the standard GLM analysis: estimate the model’s coefficients (β) and determine whether they are statistically significant. Our choices are to pick

a differencing matrix, D , and solve by ordinary least squares (OLS), or do nothing to the data (use $D = I$) and solve by generalized least squares (GLS).

As it turns out, this decision largely depends on the type of experimental paradigm and on the design matrix. Figure 14 shows a comparison between the statistical power obtained from analyzing ASL data with different amount of noise the two strategies: differencing and not differencing. In one case the data are analyzed with a Generalized Least Squares (GLS) model and not differenced. In the other case, the data are pairwise differenced and analyzed with the usual ordinary least squares (OLS).

Specifically, it shows the statistical power for no differencing with GLS and that of pairwise differencing with OLS for the 3 study designs over SNR values ranging between 0.25 and 2. The dotted lines on the random event related figure indicate ± 2 standard deviations of the average power over the 100 simulations. As expected, the power is similar between the two methods for the block design, but the “no differencing GLS” model is shown to have larger power for the event related study designs. The random event related design can have up to 14% (s.d. 0.7%) lower power when OLS is used compared to GLS. (Mumford, Hernandez-Garcia et al. 2006). An added benefit is that the GLS approach also enables us to estimate both BOLD and ASL effects simultaneously, which may be desirable in some analyses.

A final note is that the above quantification method using the GLM can be used whether the data are differenced and undifferenced, as long as the design matrix is constructed carefully to reflect the differencing scheme.

11. Challenges facing ASL

So far, we have illustrated the utility of ASL in functional MRI, but we must reiterate that ASL is not a panacea, though. Arterial spin labeling techniques pose a number of challenges. These challenges must be overcome so that ASL techniques can take a more central role in the study of brain function.

ASL is challenged by low SNR, since less than 10% of the water in a given voxel is contributed by blood (Pawlik, Rackl et al. 1981; Weiss, Buchweitz et al. 1982) and the label decays quickly. This problem can be partially alleviated by continuous arterial spin labeling, which increases the amount of label that is introduced into the tissue. Gains in the SNR have also been made with the development of pulse sequences that employ background suppression pulses, as these dramatically reduce the noise contribution from stationary tissue (Garcia, Duhamel et al. 2005). However, these background suppression pulses interfere with the ability to quantify perfusion, so they limit the measurement to relative CBF measures (Shin, Liu et al. 2011).

Another major challenge to ASL techniques is low temporal resolution because ASL measurements take from 3 to 6 seconds depending on the amount of time spent labeling the arterial blood. Collecting multi-slice data can be challenging because the imaging RF pulses can interfere with the inversion label of the arterial water (Silva, Zhang et al. 1995). Lastly, all slices must be acquired within a short period of time in order to sample the label before it clears from

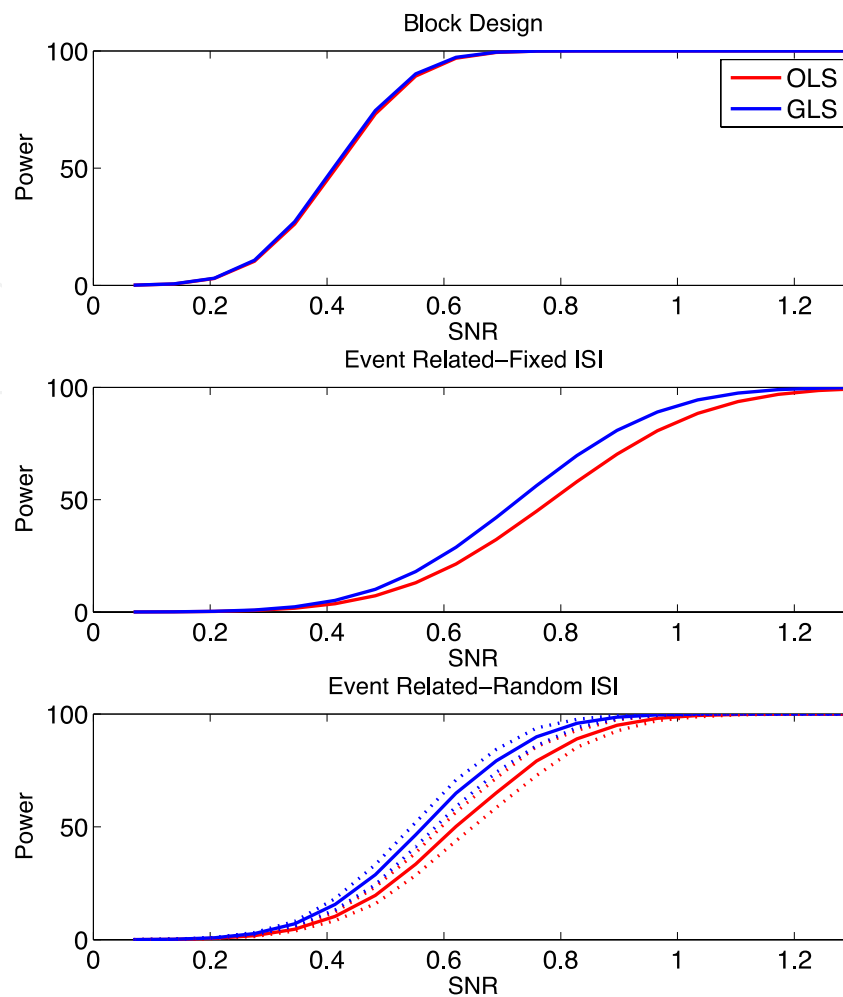


Figure 14. Whether we use an ordinary least squares (OLS) approach on differenced data or a generalized least squares approach (GLS) on raw data can make a significant difference in the statistical power of the analysis. It's not important for blocked designs, but in the case of event related designs, whose frequency content is relatively higher, it makes a significant difference. Reproduced from (Mumford, Hernandez-Garcia et al. 2006).

the tissue of interest. As we have discussed earlier, functional MRI experiments often require the ability to scan the whole brain at a rapid rate in order to localize and characterize brief, subtle changes in cerebral activity (i.e., event related experiments). Collecting multi-slice ASL images in a rapid manner is challenging, given the SNR and clearance rate of the label. While one can collect images at a rate roughly equivalent to the transit time of the subject (roughly 1.5 seconds) the number of slices at this rate is limited to less than five at the present time (Hernandez-Garcia, Lee et al. 2004; Hernandez-Garcia, Lee et al. 2005).

12. Conclusions

In this chapter we have examined arterial spin labeling as technique for functional MRI in depth. As we have seen, there are some clear advantages to collecting ASL data for functional

studies in some circumstances, but other times it may not be beneficial at all. ASL is really well suited for longitudinal studies and studies with long blocks of activation, but it may not be so well suited for event related experiments. ASL offers quantitative measures of perfusion at rest and activation. On a per subject basis, the technique's limitations are low SNR and temporal resolution, but there are significant gains in terms of population variance and contrast between resting and active states.

Author details

Luis Hernandez-Garcia and Hesamoddin Jahanian

University of Michigan, FMRI Laboratory, USA

References

- [1] Aguirre, G., J. Detre, et al. (2002). "Experimental design and the relative sensitivity of BOLD and perfusion fMRI." *Neuroimage* 15(3): 488-500.
- [2] Ances, B. M., O. Leontiev, et al. (2008). "Regional differences in the coupling of cerebral blood flow and oxygen metabolism changes in response to activation: implications for BOLD-fMRI." *Neuroimage* 39(4): 1510-1521.
- [3] Bagarinao, E., K. Matsuo, et al. (2003). "Estimation of general linear model coefficients for real-time application." *Neuroimage* 19(2): 422-429.
- [4] Bandettini, P. A., E. C. Wong, et al. (1992). "Time course EPI of human brain function during task activation." *Magn Reson Med* 25(2): 390-397.
- [5] Bernstein, M. A., K. F. King, et al. (2004). *Handbook of MRI pulse sequences*, Elsevier Academic Press.
- [6] Bevington, P. R. and D. K. Robinson (2003). *Data reduction and error analysis for the physical sciences*. Boston, McGraw-Hill.
- [7] Boynton, G., S. Engel, et al. (1996). "Linear systems analysis of functional magnetic resonance imaging in human V1." *J Neurosci* 16(13): 4207-4221.
- [8] Buxton, R. and L. Frank (1997). "A model for the coupling between cerebral blood flow and oxygen metabolism during neural stimulation." *J Cereb Blood Flow Metab* 17(1): 64-72.
- [9] Buxton, R., L. Frank, et al. (1998). "A general kinetic model for quantitative perfusion imaging with arterial spin labeling." *Magn Reson Med* 40(3): 383-396.

- [10] Buxton, R., E. Wong, et al. (1998). "Dynamics of blood flow and oxygenation changes during brain activation: the balloon model." *Magn Reson Med* 39(6): 855-864.
- [11] Caria, A., R. Veit, et al. (2007). "Regulation of anterior insular cortex activity using real-time fMRI." *Neuroimage* 35(3): 1238-1246.
- [12] Changwei, W. W., C. Kai-Hsiang, et al. (2008). "Vascular space occupancy-dependent functional MRI by tissue suppression." *Journal of Magnetic Resonance Imaging* 28(1): 219-226.
- [13] Chen, J. J., M. Wieckowska, et al. (2008). "Cerebral blood flow measurement using fMRI and PET: a cross-validation study." *International journal of biomedical imaging* 2008: 516359.
- [14] Christopher, B. G., A. S. Ronald, et al. (2009). "Estimating cerebral blood volume with expanded vascular space occupancy slice coverage." *Magnetic Resonance in Medicine* 61(5): 1193-1200.
- [15] Cohen, E. R., K. Ugurbil, et al. (2002). "Effect of basal conditions on the magnitude and dynamics of the blood oxygenation level-dependent fMRI response." *J Cereb Blood Flow Metab* 22(9): 1042-1053.
- [16] Cox, R. W., A. Jesmanowicz, et al. (1995). "Real-time functional magnetic resonance imaging." *Magn Reson Med* 33(2): 230-236.
- [17] Davis, T. L., K. K. Kwong, et al. (1998). "Calibrated functional MRI: mapping the dynamics of oxidative metabolism." *Proc Natl Acad Sci U S A* 95(4): 1834-1839.
- [18] deCharms, R. C. (2008). "Applications of real-time fMRI." *Nat Rev Neurosci* 9(9): 720-729.
- [19] deCharms, R. C., K. Christoff, et al. (2004). "Learned regulation of spatially localized brain activation using real-time fMRI." *Neuroimage* 21(1): 436-443.
- [20] Detre, J., J. Leigh, et al. (1992). "Perfusion imaging." *Magn Reson Med* 23(1): 37-45.
- [21] Duong, T., E. Yacoub, et al. (2002). "High-resolution, spin-echo BOLD, and CBF fMRI at 4 and 7 T." *Magn Reson Med* 48(4): 589-593.
- [22] Edelman, R. and Q. Chen (1998). "EPISTAR MRI: multislice mapping of cerebral blood flow." *Magn Reson Med* 40(6): 800-805.
- [23] Fernandez-Seara, M. A., J. Wang, et al. (2007). "Imaging mesial temporal lobe activation during scene encoding: comparison of fMRI using BOLD and arterial spin labeling." *Hum Brain Mapp* 28(12): 1391-1400.
- [24] Fernandez-Seara, M. A., Z. Wang, et al. (2005). "Continuous arterial spin labeling perfusion measurements using single shot 3D GRASE at 3 T." *Magn Reson Med* 54(5): 1241-1247.

- [25] Gai, N. D., S. L. Talagala, et al. (2011). "Whole-brain cerebral blood flow mapping using 3D echo planar imaging and pulsed arterial tagging." *J Magn Reson Imaging* 33(2): 287-295.
- [26] Garcia, D., C. de Bazelaire, et al. (2005). *Pseudo-continuous Flow Driven Adiabatic Inversion for Arterial Spin Labeling*. Proceedings International Society for Magnetic Resonance in Medicine, Miami, FLA.
- [27] Garcia, D. M., G. Duhamel, et al. (2005). "Efficiency of inversion pulses for background suppressed arterial spin labeling." *Magn Reson Med* 54(2): 366-372.
- [28] Gembris, D., J. G. Taylor, et al. (2000). "Functional magnetic resonance imaging in real time (FIRE): sliding-window correlation analysis and reference-vector optimization." *Magn Reson Med* 43(2): 259-268.
- [29] Gollub, R. L., H. C. Breiter, et al. (1998). "Cocaine decreases cortical cerebral blood flow but does not obscure regional activation in functional magnetic resonance imaging in human subjects." *Journal of cerebral blood flow and metabolism : official journal of the International Society of Cerebral Blood Flow and Metabolism* 18(7): 724-734.
- [30] Gu, H., H. Lu, et al. (2006). "Noninvasive quantification of cerebral blood volume in humans during functional activation." *Neuroimage* 30(2): 377-387.
- [31] Gunther, M., K. Oshio, et al. (2005). "Single-shot 3D imaging techniques improve arterial spin labeling perfusion measurements." *Magn Reson Med* 54(2): 491-498.
- [32] Haacke, E. M. (1999). *Magnetic resonance imaging : physical principles and sequence design*. New York, Wiley.
- [33] Hermes, M., D. Hagemann, et al. (2007). "Reproducibility of continuous arterial spin labeling perfusion MRI after 7 weeks." *Magma* 20(2): 103-115.
- [34] Hernandez-Garcia, L., H. Jahanian, et al. (2011). "Real-time functional MRI using pseudo-continuous arterial spin labeling." *Magnetic resonance in medicine : official journal of the Society of Magnetic Resonance in Medicine / Society of Magnetic Resonance in Medicine* 65(6): 1570-1577.
- [35] Hernandez-Garcia, L., H. Jahanian, et al. (2010). "Quantitative Analysis of Arterial Spin Labeling fMRI Data Using a General Linear Model." *Magnetic Resonance Imaging* 28(7): 919-927.
- [36] Hernandez-Garcia, L., G. R. Lee, et al. (2004). "Fast, pseudo-continuous arterial spin labeling for functional imaging using a two-coil system." *Magn Reson Med* 51(3): 577-585.
- [37] Hernandez-Garcia, L., G. R. Lee, et al. (2005). "Quantification of perfusion fMRI using a numerical model of arterial spin labeling that accounts for dynamic transit time effects." *Magn Reson Med* 54(4): 955-964.

- [38] Hernandez-Garcia, L., D. Lewis, et al. (2007). "Magnetization transfer effects on the efficiency of flow-driven adiabatic fast passage inversion of arterial blood." *NMR Biomed* 20: 733-742.
- [39] Hoge, R. D., J. Atkinson, et al. (1999). "Linear coupling between cerebral blood flow and oxygen consumption in activated human cortex." *Proceedings of the National Academy of Sciences of the United States of America* 96(16): 9403-9408.
- [40] Jaeggi, S. M., B. E. Studer, et al. (2009). *Improving Fluid Intelligence – Single N-back Is As Effective As Dual N-back*. Annual Meeting of the Psychonomic Society, Boston, MA.
- [41] Jahanian, H., D. C. Noll, et al. (2011). "B0 field inhomogeneity considerations in pseudo-continuous arterial spin labeling (pCASL): effects on tagging efficiency and correction strategy." *NMR in Biomedicine*: n/a-n/a.
- [42] Jin, T. and S.-G. Kim (2008). "Improved cortical-layer specificity of vascular space occupancy fMRI with slab inversion relative to spin-echo BOLD at 9.4T." *Neuroimage* 40(1): 59-67.
- [43] Kemeny, S., F. Q. Ye, et al. (2005). "Comparison of continuous overt speech fMRI using BOLD and arterial spin labeling." *Human Brain Mapping* 24(3): 173-183.
- [44] Kety, S. S. and C. Schmidt (1945). "THE DETERMINATION OF CEREBRAL BLOOD FLOW IN MAN BY THE USE OF NITROUS OXIDE IN LOW CONCENTRATIONS." *American Journal of Physiology*(143): 53-66.
- [45] Kim, J., J. Whyte, et al. (2006). "Continuous ASL perfusion fMRI investigation of higher cognition: quantification of tonic CBF changes during sustained attention and working memory tasks." *Neuroimage* 31(1): 376-385.
- [46] Kim, S. (1995). "Quantification of relative cerebral blood flow change by flow-sensitive alternating inversion recovery (FAIR) technique: application to functional mapping." *Magn Reson Med* 34(3): 293-301.
- [47] Kim, S. and N. Tsekos (1997). "Perfusion imaging by a flow-sensitive alternating inversion recovery (FAIR) technique: application to functional brain imaging." *Magn Reson Med* 37(3): 425-435.
- [48] Kwong, K., J. Belliveau, et al. (1992). "Dynamic magnetic resonance imaging of human brain activity during primary sensory stimulation." *Proc Natl Acad Sci U S A* 89(12): 5675-5679.
- [49] Lassen, N. A. and W. Perl (1979). *Tracer kinetic methods in medical physiology*. New York, Raven Press.
- [50] Leontiev, O. and R. B. Buxton (2007). "Reproducibility of BOLD, perfusion, and CMRO2 measurements with calibrated-BOLD fMRI." *Neuroimage* 35(1): 175-184.
- [51] Liu, T. and E. Wong (2005). "A signal processing model for arterial spin labeling functional MRI." *Neuroimage* 24(1): 207-215.

- [52] Lu, H., M. Law, et al. (2005). "Novel approach to the measurement of absolute cerebral blood volume using vascular-space-occupancy magnetic resonance imaging." *Magn Reson Med* 54(6): 1403-1411.
- [53] Lund, T., K. Madsen, et al. (2006). "Non-white noise in fMRI: does modelling have an impact?" *Neuroimage* 29(1): 54-66.
- [54] Mulderink, T. A., D. R. Gitelman, et al. (2002). "On the use of caffeine as a contrast booster for BOLD fMRI studies." *Neuroimage* 15(1): 37-44.
- [55] Mumford, J. A., L. Hernandez-Garcia, et al. (2006). "Estimation efficiency and statistical power in arterial spin labeling fMRI." *Neuroimage* 33(1): 103-114.
- [56] Nakai, T., E. Bagarinao, et al. (2006). "Dynamic monitoring of brain activation under visual stimulation using fMRI--The advantage of real-time fMRI with sliding window GLM analysis." *Journal of Neuroscience Methods* 157(1): 158-167.
- [57] Nencka, A. S. and D. B. Rowe (2007). "Reducing the unwanted draining vein BOLD contribution in fMRI with statistical post-processing methods." *Neuroimage* 37(1): 177-188.
- [58] O'Gorman, R. L., V. Kumari, et al. (2006). "Personality factors correlate with regional cerebral perfusion." *Neuroimage* 31(2): 489-495.
- [59] Olafsson, V. T., D. C. Noll, et al. (2008). "Fast Joint Reconstruction of Dynamic R2* and Field Maps in Functional MRI." *Medical Imaging, IEEE Transactions on* 27(9): 1177-1188.
- [60] Olson, I. R., H. Rao, et al. (2006). "Using perfusion fMRI to measure continuous changes in neural activity with learning." *Brain and Cognition* 60(3): 262-271.
- [61] Pawlik, G., A. Rackl, et al. (1981). "Quantitative capillary topography and blood flow in the cerebral cortex of cats: an in vivo microscopic study." *Brain Res* 208(1): 35-58.
- [62] Pfeuffer, J., G. Adriany, et al. (2002). "Perfusion-based high-resolution functional imaging in the human brain at 7 Tesla." *Magn Reson Med* 47(5): 903-911.
- [63] Phan, K. L., D. A. Fitzgerald, et al. (2004). "Real-time fMRI of cortico-limbic brain activity during emotional processing." *Neuroreport* 15(3): 527-532.
- [64] Posse, S., D. Fitzgerald, et al. (2003). "Real-time fMRI of temporolimbic regions detects amygdala activation during single-trial self-induced sadness." *NeuroImage* 18: 760-768.
- [65] Rao, H., S. J. Gillihan, et al. (2007). "Genetic variation in serotonin transporter alters resting brain function in healthy individuals." *Biological Psychiatry* 62(6): 600-606.
- [66] Rao, H., J. Wang, et al. (2007). "Imaging brain activity during natural vision using CASL perfusion fMRI." *Human Brain Mapping* 28(7): 593-601.

- [67] Raoult, H., J. Petr, et al. (2011). "Arterial spin labeling for motor activation mapping at 3T with a 32-channel coil: Reproducibility and spatial accuracy in comparison with BOLD fMRI." *Neuroimage* 58(1): 157-167.
- [68] Shin, D., H. Liu, et al. (2011). *Effect of background suppression on CBF quantitation in pseudo continuous arterial spin labeling*. International Society for Magnetic Resonance in Medicine, Montreal, QC, Canada.
- [69] Silva, A., W. Zhang, et al. (1995). "Multi-slice MRI of rat brain perfusion during amphetamine stimulation using arterial spin labeling." *Magn Reson Med* 33(2): 209-214.
- [70] Smith, A. M., B. K. Lewis, et al. (1999). "Investigation of Low Frequency Drift in fMRI Signal." *Neuroimage* 9(5): 526-533.
- [71] Talagala, S., F. Ye, et al. (2004). "Whole-brain 3D perfusion MRI at 3.0 T using CASL with a separate labeling coil." *Magn Reson Med* 52(1): 131-140.
- [72] Tjandra, T., J. C. W. Brooks, et al. (2005). "Quantitative assessment of the reproducibility of functional activation measured with BOLD and MR perfusion imaging: Implications for clinical trial design." *Neuroimage* 27(2): 393-401.
- [73] Vazquez, A. and D. Noll (1998). "Nonlinear aspects of the BOLD response in functional MRI." *Neuroimage* 7(2): 108-118.
- [74] Vazquez, A. L., G. R. Lee, et al. (2006). "Application of selective saturation to image the dynamics of arterial blood flow during brain activation using magnetic resonance imaging." *Magn Reson Med* 55(4): 816-825.
- [75] Voyvodic, J. T. (1999). "Real-time fMRI paradigm control, physiology, and behavior combined with near real-time statistical analysis." *Neuroimage* 10(2): 91-106.
- [76] Wang, J., G. Aguirre, et al. (2003). "Empirical analyses of null-hypothesis perfusion FMRI data at 1.5 and 4 T." *Neuroimage* 19(4): 1449-1462.
- [77] Wang, J., G. Aguirre, et al. (2003). "Arterial spin labeling perfusion fMRI with very low task frequency." *Magn Reson Med* 49(5): 796-802.
- [78] Wang, J., G. K. Aguirre, et al. (2003). "Arterial spin labeling perfusion fMRI with very low task frequency." *Magn Reson Med* 49(5): 796-802.
- [79] Wang, J., D. Alsop, et al. (2002). "Comparison of quantitative perfusion imaging using arterial spin labeling at 1.5 and 4.0 Tesla." *Magn Reson Med* 48(2): 242-254.
- [80] Wang, J., H. Rao, et al. (2005). "Perfusion functional MRI reveals cerebral blood flow pattern under psychological stress." *Proceedings of the National Academy of Sciences of the United States of America* 102(49): 17804-17809.
- [81] Wang, J., Y. Zhang, et al. (2005). "Amplitude-modulated Continuous Arterial Spin-labeling 3.0-T Perfusion MR Imaging with a Single Coil: Feasibility Study." *Radiology* 235(1): 218-228.

- [82] Weiss, H., E. Buchweitz, et al. (1982). "Quantitative regional determination of morphometric indices of the total and perfused capillary network in the rat brain." *Circ Res* 51(4): 494-503.
- [83] Williams, D., J. Detre, et al. (1992). "Magnetic resonance imaging of perfusion using spin inversion of arterial water." *Proc Natl Acad Sci U S A* 89(1): 212-216.
- [84] Wise, R. G. and I. Tracey (2006). "The role of fMRI in drug discovery." *Journal of magnetic resonance imaging : JMRI* 23(6): 862-876.
- [85] Wong, E., R. Buxton, et al. (1997). "Implementation of quantitative perfusion imaging techniques for functional brain mapping using pulsed arterial spin labeling." *NMR Biomed* 10(4-5): 237-249.
- [86] Wong, E., R. Buxton, et al. (1998). "Quantitative imaging of perfusion using a single subtraction (QUIPSS and QUIPSS II)." *Magn Reson Med* 39(5): 702-708.
- [87] Wong, E., R. Buxton, et al. (1998). "A theoretical and experimental comparison of continuous and pulsed arterial spin labeling techniques for quantitative perfusion imaging." *Magn Reson Med* 40(3): 348-355.
- [88] Wu, W. C., M. Fernandez-Seara, et al. (2007). "A theoretical and experimental investigation of the tagging efficiency of pseudocontinuous arterial spin labeling." *Magn Reson Med* 58(5): 1020-1027.
- [89] Yoo, S. S., T. Fairney, et al. (2004). "Brain-computer interface using fMRI: spatial navigation by thoughts." *Neuroreport* 15(10): 1591-1595.
- [90] Yoo, S. S. and F. A. Jolesz (2002). "Functional MRI for neurofeedback: feasibility study on a hand motor task." *Neuroreport* 13(11): 1377-1381.
- [91] Zhang, W., A. Silva, et al. (1995). "NMR measurement of perfusion using arterial spin labeling without saturation of macromolecular spins." *Magn Reson Med* 33(3): 370-376.

IntechOpen